

Article

# Tectonic Subsidence on the East China Coast Recorded by Magnetic Properties of Pliocene Red Clay in the Yangtze Delta

Xianbin Liu <sup>1,2</sup>, Jing Chen <sup>2</sup>, Liping Xu <sup>3</sup>, Xiaoli Sun <sup>4</sup>, Lei Tan <sup>1</sup>, Minghao Lv <sup>1</sup> and Jian Song <sup>1,\*</sup>

<sup>1</sup> School of Resource and Environmental Engineering, Ludong University, Yantai 264025, China; liuxb\_801@163.com (X.L.); tanl971220@163.com (L.T.); lvminghao0513@gmail.com (M.L.)

<sup>2</sup> State Key Laboratory for Estuarine and Coastal Research, East China Normal University, Shanghai 200241, China; jchen@geo.ecnu.edu.cn

<sup>3</sup> Pilot National Laboratory for Marine Science and Technology, Qingdao 266237, China; lpxu@qnlm.ac

<sup>4</sup> Shandong Zhengyuan Digital City Construction Company, Yantai 264025, China; shdsunxiaoli@126.com

\* Correspondence: songjian04@163.com

**Abstract:** Thick red clay in northern China contains rich information about the uplifting of the Qinghai–Tibet Plateau, the drying process of Asian inland, the East Asian monsoon changes, and global cooling since 22 Ma. In comparison, the red clay widely distributed in southern China is generally much younger (<1 million years), thus limiting the paleoclimate and paleoenvironment reconstruction over a longer geological time. We conducted a comprehensive magnetic investigation on the Pliocene red clay of the core LQ11, located in the Yangtze Delta, to reveal its paleoclimate and paleoenvironment implications for the eastern China coast. Our results revealed that the Pliocene red clay in the Yangtze Delta has higher S-ratio and lower HIRM (Hard isothermal remanent magnetizations) values than Quaternary vermiculate red clay of hot–humid climate origin in southern China. This indicates a weaker transformation from maghemite to hematite during the process of pedogenesis. The lack of net-like white veins in the Pliocene red clay also indicates a relatively low intensity of pedogenesis. We believe that the Pliocene red clay, which is presently 250 m below the mean sea level, was formed in high-altitude topography before the Quaternary period, where paedogenic intensity was remarkably low. This finding shows rapid tectonic subsidence occurring on the eastern China coast since the late Pliocene and enriches the theoretical research on paleoenvironment reconstruction based on red clay.

**Keywords:** Pliocene; magnetic properties; paleoenvironment; East Asian monsoon; Yangtze Delta



**Citation:** Liu, X.; Chen, J.; Xu, L.; Sun, X.; Tan, L.; Lv, M.; Song, J. Tectonic Subsidence on the East China Coast Recorded by Magnetic Properties of Pliocene Red Clay in the Yangtze Delta. *J. Mar. Sci. Eng.* **2024**, *12*, 66. <https://doi.org/10.3390/jmse12010066>

Academic Editor: Gemma Aiello

Received: 19 October 2023

Revised: 19 December 2023

Accepted: 23 December 2023

Published: 27 December 2023



**Copyright:** © 2023 by the authors. Licensee MDPI, Basel, Switzerland. This article is an open access article distributed under the terms and conditions of the Creative Commons Attribution (CC BY) license (<https://creativecommons.org/licenses/by/4.0/>).

## 1. Introduction

The red clay, also named red soil or red earth, is widely distributed in northern and southern China and is an ideal sediment archive for exploring the late Cenozoic climate and environmental evolution (Figure 1a). The red clay underlain by the Quaternary loess in northern China was formed in Miocene–Pliocene and provides key insights into the onset of East Asian monsoons, the uplift of the Tibetan Plateau, and related desertification of the Asian interior since 22 Ma [1–3]. In comparison, the red clay in southern China, covering an area of  $20 \times 10^5$  km<sup>2</sup>, is generally composed of—from the bottom to the top—yellow vermiculated earth, uniform red clay, and brown earth [4]. The red clay in the southern regions contains abundant Palaeolithic sites harbouring rich information on human evolution. However, its deposition began about one million years ago and is much younger than that in northern China, thus limiting, to a certain extent, the reconstruction of the paleoenvironment in the subtropical and tropical areas of Asia [5,6].

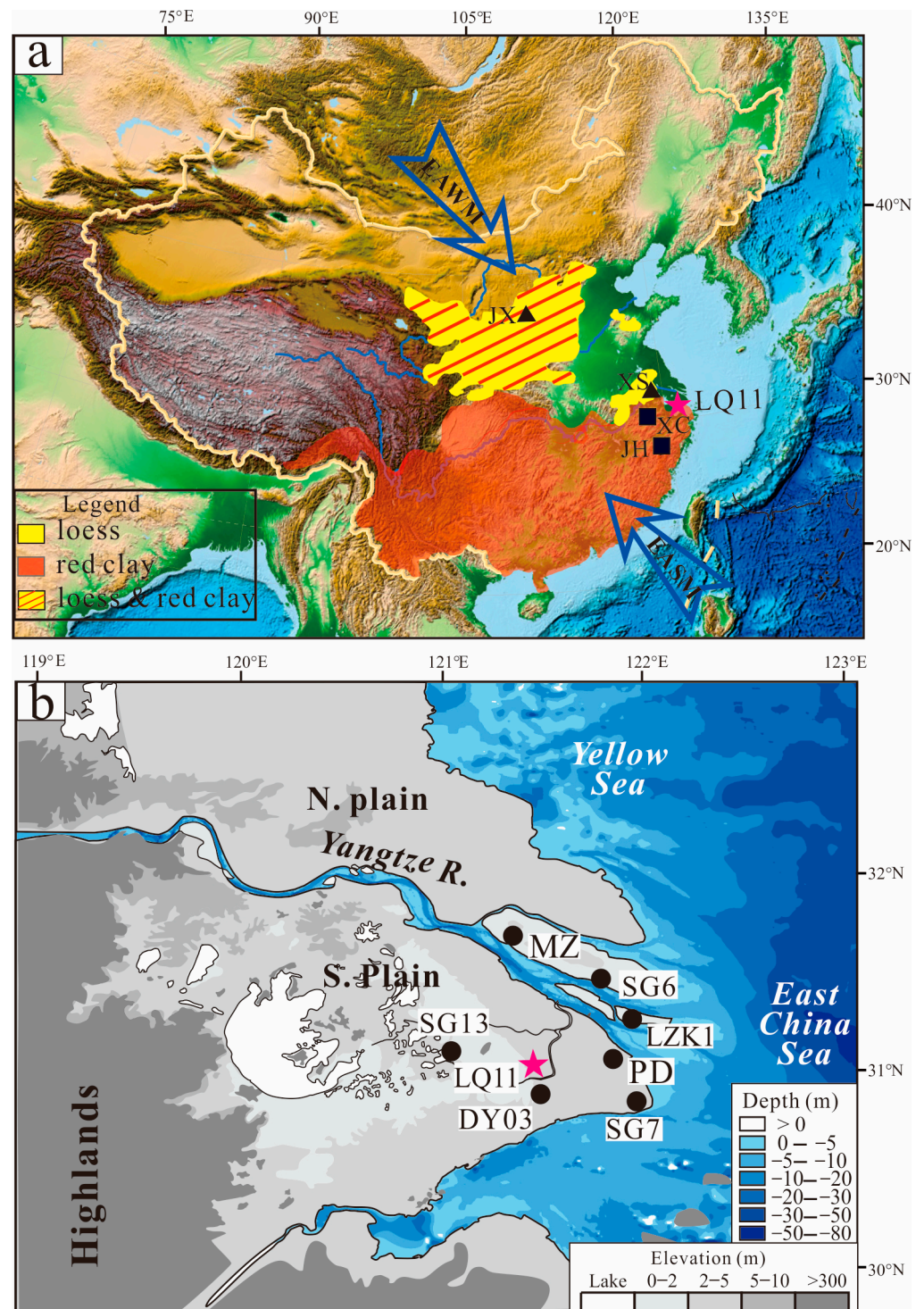


**Figure 1.** (a) Map showing the distributions of Neogene red clay and Quaternary loess in northern China and Quaternary red clay in southern China. EASM: East Asia summer monsoon; EAWM: East Asia winter monsoon. The location of the sampling site (star); Tertiary red clay sections (triangle; JX: Jiaxian) in northern China, and Quaternary red clay sections (diamond; XS: Xiashu; XC: Xuancheng; JH: Jinhua) in southern China. (b) The topography of the Yangtze Delta and its surrounding areas; the cores distributed in the Yangtze Delta.

The magnetic properties of rocks and sediments are sensitive to environmental changes and are described in different research fields, such as magnetostratigraphy, palaeomagnetism, and environmental magnetism. Environmental magnetism investigates the formation, transport, deposition, and post-depositional alteration processes of magnetic minerals under various environmental conditions. [7–11]. For Neogene red clay in northern China, ultrafine magnetic minerals (maghemite) produced during pedogenesis enhance the magnetic susceptibility ( $\chi_{lf}$ ) of sediments under warm and wet climates [12]. The red clay in southern China, especially vermiculate red clay, has experienced a much stronger pedogenesis with higher temperature and rainfall than that in northern China, and more pedogenic maghemite has been transformed into hematite [13,14]. As recorded by the variations in magnetic properties, the red clay from both northern and southern China documented the evolution of the paleoenvironment in Asia, especially the East Asian paleomonsoon [13–17].

We recently discovered red clay from the Pliocene age in a 301-m-long sediment core LQ11 in the Yangtze Delta, with a buried depth greater than 250 m, which is younger than that in northern China, but older than in southern China (Figure 1b). Here, we analyse the magnetic properties of the Pliocene red clay and further reveal its paleoclimate and paleoenvironment implications by comparing it with Neogene red clay in northern China and Quaternary red clay in southern China.

## 2. Geographic Background

The Yangtze River, one of the longest rivers (>6300 km) in the world, originates from the Tibetan Plateau and flows into the East China Sea [18]. The Yangtze River Delta is located between 30°20' to 32°30' N and 119°24' to 122°30' E. It borders the Yellow Sea and East China Sea to the east and is bounded by the Tianmu Mountain and Maoshan to the west. The northern boundary is marked by the line connecting Yangzhou City, Taizhou City, and Rudong City, while the southern boundary is defined by the northern shore of Hangzhou Bay.

The predominant bedrock in the Yangtze Delta region is composed of igneous rocks that were formed from the Neoproterozoic to the Late Cenozoic. Among them, the Late Jurassic and Cretaceous igneous rocks have the widest distributions, accounting for more than two-thirds of the total bedrock area. The residual hills exposed in the southern region are also of igneous origin. Sedimentary rocks are scattered and include sandstone, tuffaceous limestone, and volcanic breccia. Metamorphic rocks have the smallest distribution area in the region and are only found in the southern areas.

The extent of marine transgression in the Yangtze River estuary region reached its maximum 8000–7000 years ago [18]. The sea level then remained relatively stable, resulting in the accumulation of a large amount of sediment carried by the Yangtze River into the estuarine area. This caused the coastline to steadily advance seaward, gradually forming the modern delta.

The delta has low-lying topography, with an average elevation of about 4 m. Apart from a few exposed bedrock hills in the southern region, the majority of the Yangtze Delta is characterized by a cover of thick and loosely deposited sediments that are in unconformable contact with the underlying Mesozoic intermediate-acidic igneous bedrock. Pliocene strata are found only in sporadic depressions, typically with a thickness of less than 40 m. Moving into the Quaternary period, the strata reach their maximum thickness along the east coast, exceeding 300 m, and gradually thin out and disappear towards the west.

## 3. Materials and Methods

A 301 metre long and continuous sediment core (LQ11) was taken from the Yangtze delta (Figure 1b). A total of 277 samples from the whole core, including 19 samples in the Pliocene strata, were collected for measurement (Table 1).

**Table 1.** Sampling depth and sediment granularity.

Sample No.	Depth (m)	Clay (%)	Silt (%)	Sand (%)	Md ( $\mu\text{m}$ )
LQ11-1	301	27.40	61.90	10.70	24.34
LQ11-2	300	44.60	54.50	0.90	14.75
LQ11-3	297	40.10	59.89	0.01	8.08
LQ11-4	295	33.60	61.00	5.40	21.13
LQ11-5	292.5	38.30	60.00	1.70	11.14
LQ11-6	288	57.40	42.50	0.10	6.88
LQ11-7	285	56.60	43.20	0.20	7.20
LQ11-8	284	25.60	68.90	5.50	19.77
LQ11-9	282.5	30.50	63.80	5.70	19.43
LQ11-10	280	60.00	40.00	0.00	6.64
LQ11-11	276.5	30.10	62.30	7.60	21.13
LQ11-12	273.5	35.20	58.70	6.10	20.38
LQ11-13	270.8	36.90	57.50	5.60	19.11
LQ11-14	268	44.70	54.70	0.60	12.17
LQ11-15	265.5	26.70	64.90	8.40	24.46
LQ11-16	262	36.20	56.00	7.80	20.71
LQ11-17	257.5	24.20	71.00	4.80	18.32
LQ11-18	255	32.60	64.20	3.20	14.39
LQ11-19	253.2	35.40	59.00	5.60	17.83

Magnetic susceptibility ( $\chi_{lf}$  and  $\chi_{hf}$ ) was measured using a Bartington MS2. After being demagnetized with a Dtech2000 (maximum alternating magnetic field: 100 mT, direct current magnetic field: 0.04 mT) to obtain non-hysteretic remanent magnetization, the sample was placed in a Minispin magnetometer to measure its remanent magnetization. Saturation isothermal remanent magnetization (IRM) was obtained using an MMPM10 pulse magnetometer at a 1 T magnetic field. S-ratio was calculated as  $-\text{IRM} - 300 \text{ mT}/\text{SIRM}$ , and HIRM =  $(\text{SIRM} - \text{IRM} - 300 \text{ mT})/2$ .

Based on the above parameters of the samples at room temperature, typical samples were selected for hysteresis loop and thermal demagnetization curve measurements using a variable field magnetic balance (VFTB). First-order reversal curve (FORC) was performed with a MicroMag3902 gradient magnetometer.

Four typical samples were selected to extract magnetic minerals, perform mineral morphology scanning, and measure the energy spectrum. The scanning electron microscope used was a JEOL JSM4800F field emission scanning electron microscope, and the energy spectrum testing instrument used was an Oxford Instruments X-ray energy spectrum analyser. Particle size testing was performed using a Coulter LS-100Q laser particle size analyser (measuring range: 0.02–2000  $\mu\text{m}$ ).

## 4. Results

### 4.1. Lithology of the Core LQ11

The LQ11 borehole recorded the Gauss, Matuyama, and Bruhess polarities based on a comparison of the magnetic inclination changes with a standard polarity column [19]. The boundaries of the three polarities were marked at 252 m and 112 m, where the section above 252 m is characterized by Gauss normal polarity, the strata between 252 m and 112 m exhibits Matuyama reverse polarity, and the interval from 112 m to the top of the borehole corresponds to Bruhess normal polarity.

The regional bedrock present below the red clay was Mesozoic basalt. The Pliocene red clay, found at depths between 301 and 252.7 m, is unconformably positioned on the regional bedrock (Figures 2 and 3). Within the layers of the Early Pleistocene period (252.7–112 m) are noticeable occurrences of four sedimentary cyclothem. These are characterized by a base of grey gravelly sand and coarse sand, which are subsequently covered by layers of brown silt. Moving into the Middle Pleistocene strata (112–67.6 m), there is an observable pattern of alternating strata. These comprise layers of gravelly sand along with various

grades of sand, ranging from coarse to fine. Transitioning to the late Pleistocene strata (67.6–41.3 m), distinct thick cyclic units become apparent and are predominantly composed of greyish coarse sand and silt. The Holocene strata, spanning from 41.3 to 0 m, are characterized by deposits of fine sand and clayey silt.

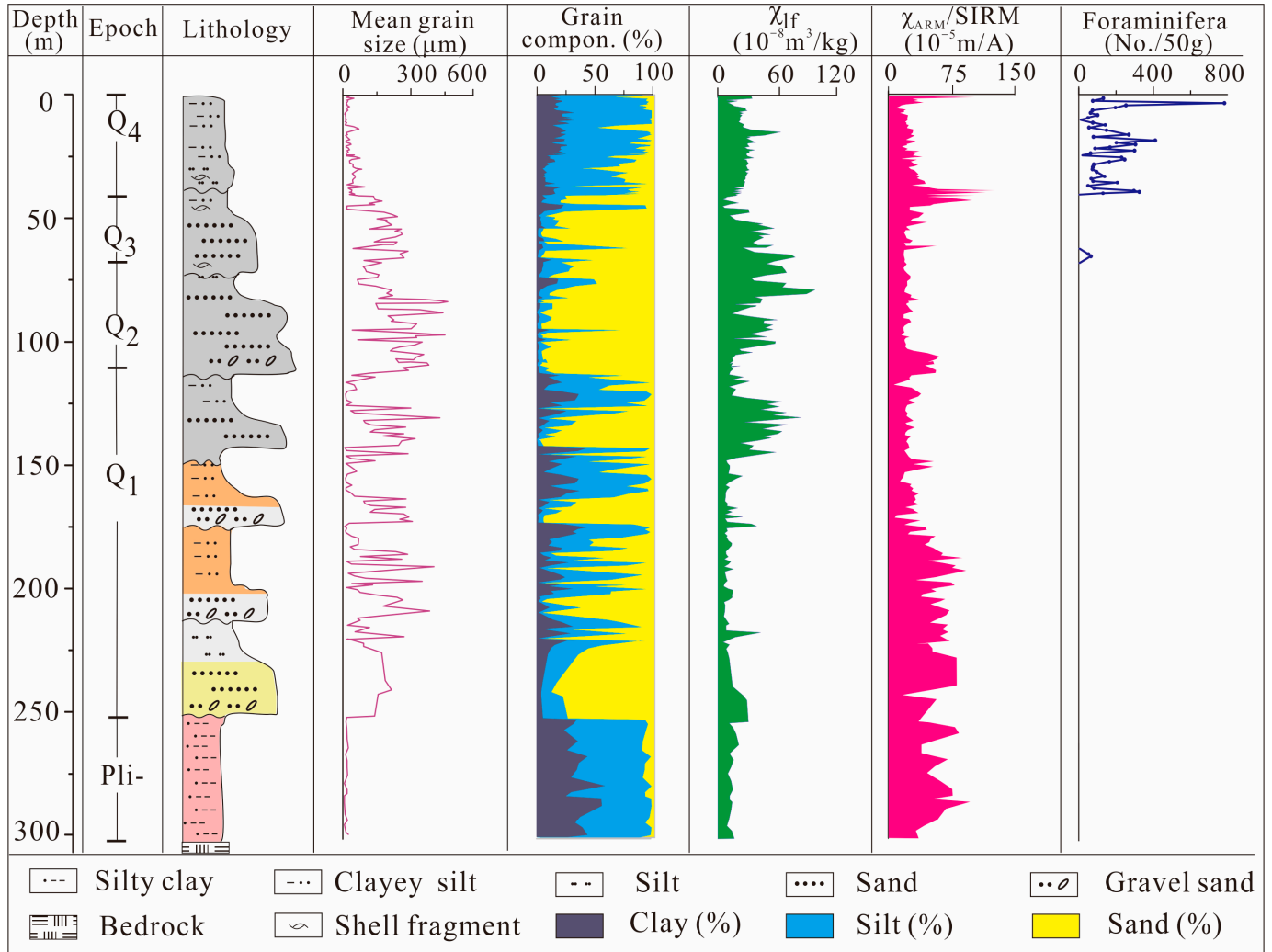


**Figure 2.** Lithology, mean grain size, abundance of foraminifera, and magnetic properties of the core LQ11.

#### 4.2. Magnetic Properties of Pliocene Red Clay in Core LQ11

Generally, the magnetic parameters of Pliocene red clay in core LQ11 exhibit small down-core fluctuations (Figure 4). The  $\chi_{lf}$  is lower than  $21.18 \times 10^{-8} \text{ m}^3\text{kg}^{-1}$ , and SIRM ranges from  $615.09$  to  $2623.45 \times 10^{-5} \text{ Am}^2\text{kg}^{-1}$ , which means that there are fewer ferri-magnetic minerals in the clay [7].  $\chi_{fd}\%$  is generally lower than 5%, indicating the small contribution of viscous superparamagnetic particles (VSP,  $\sim 0.02 \text{ }\mu\text{m}$ ) of magnetic grains to the susceptibility signal. Low values of  $\chi_{ARM}$  and  $\chi_{ARM}/\chi_{lf}$  imply low concentrations of single-domain magnetic minerals [8]. The S-ratios are all less than 0.8, indicating a high proportion of hard magnetic minerals.



**Figure 3.** Lithology photos of the Pliocene strata in the core LQ11. Below 301 m, consists of a bedrock of black basalt; 301–252.7 m represents the Pliocene strata; and the lower stratum (301–283.5 m) is mostly dark red, while the upper section (283.5–252.7 m) is bright red, with the presence of calcareous nodules; above 252.7 m, consists of the Quaternary strata, yellow-brown coarse sand, and a mixture of gravel and clay.

The thermomagnetic curves, hysteresis loops, and FORC diagrams obtained from the two representative samples exhibit similar patterns, indicating the presence of the same magnetic minerals in the red clay (Figure 5). A small convex shape observed in the heating curve between 150 °C and 300 °C suggests the formation of maghemite from Fe-hydroxides such as goethite. A significant decrease in magnetization occurs before reaching 580 °C, indicating the widespread occurrence of magnetite (Figure 5a,d). Slight decreases in magnetization up to 680 °C suggest the presence of hematite (Figure 5a,d). The raw and dia/para-corrected hysteresis loops display noticeable differences, which can be attributed to contributions from paramagnetic or diamagnetic components (Figure 5b,e). The corrected loops exhibit a characteristic wasp-waisted shape and do not close until a field strength of 1000 mT is reached. This behaviour is often associated with the coexistence of two magnetic components with distinctly different coercivities (Figure 5b,e). The FORC diagrams provide valuable insights into the magnetic properties of the samples. Along the  $H_u$  axis (>60 mT), the contours show a greater degree of divergence, indicating a wider range of coercivity values. On the other hand, along the  $H_c$  axis (<80 mT) is a distribution of low coercivity values. These features suggest that the samples are dominated by multi-domain (MD) magnetite grains (Figure 5c,f).

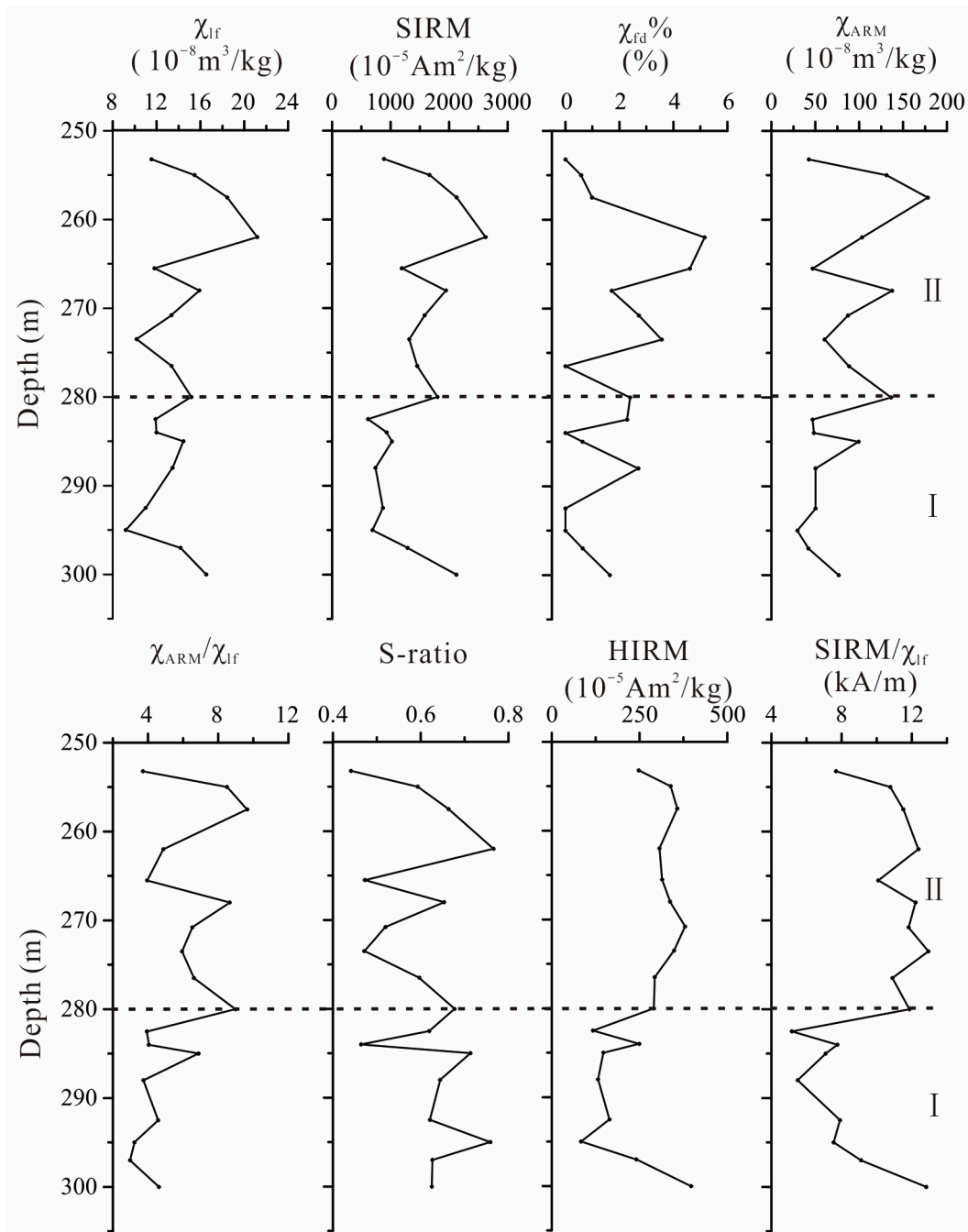


**Figure 4.** Magnetic parameters, including  $\chi_{lf}$ , SIRM,  $\chi_{fd}\%$ ,  $\chi_{ARM}$ ,  $\chi_{ARM}/\chi_{lf}$ , S-ratios, HIRM, and SIRM/ $\chi_{lf}$ , of the Pliocene red clay.

To determine the specific magnetic minerals present, we conducted SEM observations and EDS analyses on representative samples' magnetic extracts. The SEM images revealed that the magnetic particles consist of irregularly shaped iron oxides, such as magnetite and hematite, which is also revealed by the high peaks of O and Fe on the EDS spectra (Figure 6).

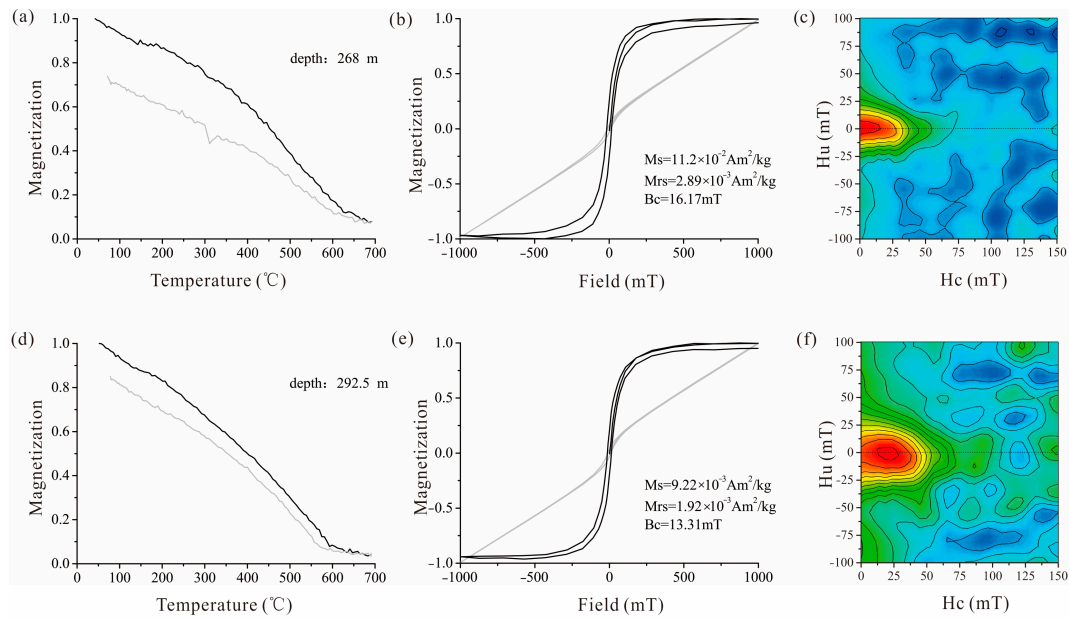


**Figure 5.** Magnetic properties of representative samples at depths of 268 and 292.5 m. (a,d), thermomagnetic curves; (b,e), black: heating curves; grey: cooling curves), hysteresis loops; (c,f), FORC diagrams.

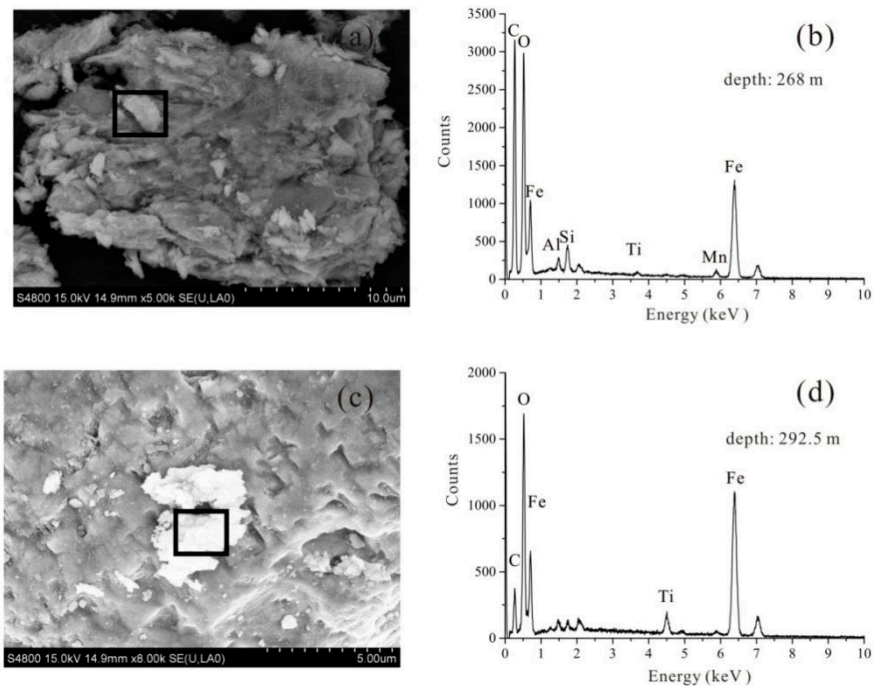


**Figure 6.** SEM images (a,c) and EDS spectra (b,d) of representative samples at depths of 268 and 292.5 m, respectively. Under the scanning electron microscope, magnetic minerals exhibit irregular shapes, smooth surfaces, and relatively large particles.

## 5. Discussion

### 5.1. Main Controlling Role of the Magnetic Properties of Pliocene Red Clay

The magnetic minerals may originate from detrital, biogenic, or authigenic sources [8]. Biogenic magnetite or greigite, typically formed through magnetotactic bacteria’s biomineralization process, usually exhibits a single domain size (SD). In the FORC diagram, this type of mineral would be characterized by a narrow vertical spread along the  $H_u$  axis ( $<20$  mT) and a wide horizontal spread along the  $H_c$  axis [19]. However, no iron sulphides were detected in the Pliocene red clay, which is supported by their low SIRM/ $\chi$  values, the

presence of divergent contours in the FORC diagram, and the absence of an S peak in the EDS spectra (Figure 5). Authigenic iron sulphides are formed through post-depositional reductive diagenesis. However, no iron sulphides are detected in the Pliocene red clay, which is supported by their low SIRM/ $\chi$  values, a FORC diagram characterized by more divergent contours along the  $H_u$  axis, and no S peak in the EDS spectra (Figures 4–6). The total organic matter content is generally low, likely minimizing the vulnerability of the sediment to reductive dissolution (Table 2). Therefore, the magnetic minerals in Pliocene red clay were mainly of detrital origin.

**Table 2.** Magnetic susceptibility, mean grain size,  $TiO_2/Al_2O_3$ , and TOC values of representative samples.

Depth (m)	$\chi_{lf}$ ( $10^{-8} \text{ m}^3 \text{ kg}^{-1}$ )	Md ( $\mu\text{m}$ )	$TiO_2/Al_2O_3$	TOC (%)
295	9.18	21.13	0.070	0.33
285	14.45	7.20	0.063	0.30
270.8	13.36	19.11	0.068	0.27
255	15.45	14.39	0.066	0.25

Either wind-blown dust or terrigenous materials (soil) from local catchments could be potential sources of detrital sediments. The magnetic properties of the sediments are different from those in the northern Chinese Loess Plateau (Figure 7). Therefore, the magnetic minerals of sediments are probably derived from the soil of local catchments, which is also supported by the surrounding cores in terms of their magnetic, heavy minerals, and geochemical proxies [20,21].

Although there were slight differences in the magnetic properties in the upper part of the core, the provenance of red clay did not change significantly during the Pliocene era (Figure 4). This is supported by its stable Ti/Al ratios, which are widely used as a provenance indicator for various sediments [22,23]. Therefore, the Pliocene red clay can shed light on our understanding of the local paleoclimate and paleoenvironmental changes in the Yangtze Delta.

### 5.2. High Altitude Formation of Pliocene Red Clay

Maghemite is a transitional mineral, from ferrihydrite to haematite, during pedogenesis processes in soil [24,25]. As the degree of pedogenesis increases, more paedogenic maghemite is transformed into haematite [26]. The transformation of maghemite to haematite during a strong pedogenesis process played a crucial role in the magnetic depletion of the Quaternary vermiculate red clay in the Xuancheng (XC), Jinhua (JH), and Qiyang (QY) sections of southern China [13,27,28]. Therefore, magnetic parameters such as S-ratios and HIRM, which reflect the relative content of haematite, can be used to estimate the degree of paedogenic processes. Compared with Quaternary vermiculate red clay in southern China, Pliocene red clay generally has higher S-ratios and lower HIRM values, suggesting lower concentrations of haematite and intensity of pedogenesis (Figure 7d).

The Quaternary red clay in southern China generally consists of—from the bottom to the top—yellow vermiculated earth, uniform red clay, and brown earth. The net-like white veins in the Vermiculated earth resulted from iron depletion under high temperatures and abundant rainfall conditions, implying an extreme East Asian summer monsoon [29]. However, the net-like white veins were not observed in the Pliocene red clay of the core LQ11 (Figure 3), probably reflecting a temperate and slightly dry climate in the Yangtze Delta during the Pliocene, and that the Pliocene red clay had undergone a relatively low intensity of pedogenesis.

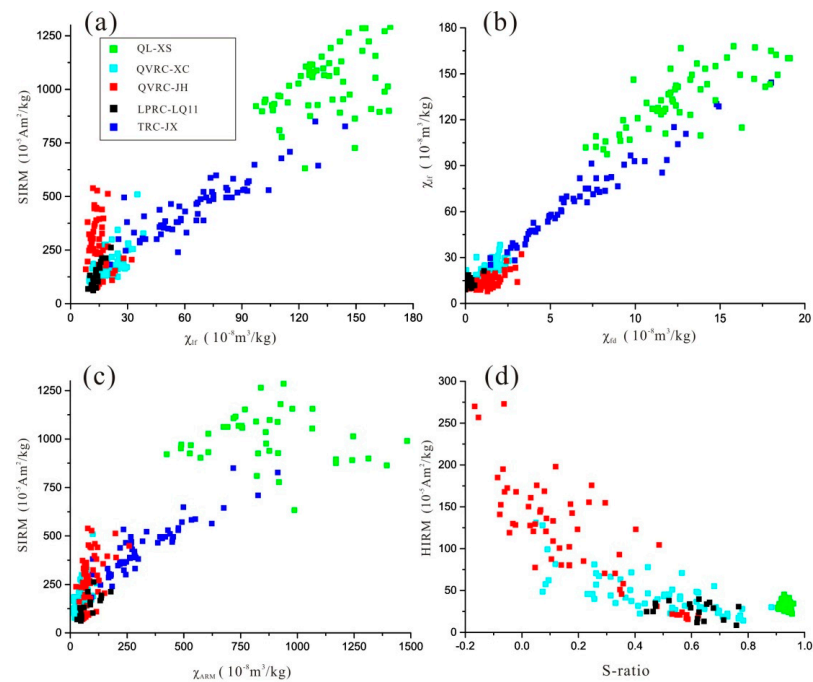


**Figure 7.** Magnetic properties of sediments from different strata, including Tertiary red clay from Jiaxian (TRC-JX) in northern China [30], and Quaternary loess from Xiashu (QL-XS) [31], Quaternary vermiculate red clay from Jinhua (QVRC-JH) [28], Xuancheng (QVRC-XC) [32], and Pliocene red clay of the core LQ11 (LPRC-LQ11) in southern China.

Pedogenesis, the process of soil formation, often influences the magnetic properties of the soil through the transformation of magnetic iron oxides [7]. The degree of chemical weathering and pedogenesis in East Asia are generally controlled by the local climate and are closely associated with monsoon intensity [33]. Thick and continuous Quaternary Loess–Neogene red clay sequences on the Chinese Loess Plateau preserve high-resolution archives for fluctuations of the East Asian monsoon during the late Cenozoic. Paedogenic ultrafine (nanoscale) magnetite/maghemite in warm and humid conditions enhanced the magnetic properties of sediments significantly, and thus magnetic parameters such as  $\chi_{lf}$  were widely used to interpret the effect of environmental and climatic change on the Chinese Loess Plateau. Magnetic records combined with geochemical data from a series of sections indicate that the summer monsoon intensity has been enhanced since 8 Ma and reached a maximum in 4.5–2.6 Ma, possibly due to tectonic events such as the phased uplift of the Tibetan Plateau [34]. Due to global cooling, the summer monsoon initiated a weakening trend in East Asia after 2.6 Ma [1]. Consistent trends of summer monsoon are also recorded in the depositional sequences of the South China Sea, as indicated by clay minerals and terrigenous mass accumulation rate at Ocean Drilling Program (ODP) Site 1146, 1148 [35,36]. Although the strength and time of the East Asian summer monsoon has varied over the long geologic time, it has commonly been accepted that the Pliocene era was warmer and wetter than the Quaternary era [37–41]. Correspondingly, stronger chemical weathering and pedogenesis in both the Chinese Loess Plateau and South China Sea generally occurred in Pliocene sediments than in Quaternary sediments [41,42]. However, the pedogenesis of sediments in the Yangtze Delta differed, and the Pliocene red clay underwent a relatively low intensity of pedogenesis. The Yangtze Delta was probably at a high altitude during the Pliocene, resulting in weak weathering of sediments, which further limited the transformation from maghemite to haematite during pedogenesis.

### 5.3. Tectonic Subsidence of the Yangtze Delta during the Quaternary Period

The evolution of the sedimentary environment of the Yangtze Delta during the late Cenozoic period goes together with continuous Neo-tectonic subsidence, and climate

and sea level changes [43]. Detailed sedimentary research from hundreds of boreholes revealed that either alluvial fan or lacustrine facies occurred in Pliocene stratigraphy in some areas, and some boreholes even lack Pliocene deposition, indicating a great difference in altitude in the region, and consequently, depositional and erosion areas coexisted in the south plain of Yangtze delta during the Pliocene period (Figure 8). *Picea* and *Abies* pollen, which are indicators of cold climate, remained at relatively stable proportions in Pliocene stratigraphy, implying high-elevation landforms and a slightly dry climate in the lower Yangtze regions [44]. In the early Pleistocene, the stratigraphic layers did not contain marine biotic fossils, and the depositional environment was characterized by alluvial and fluvial facies. The sediment consists mainly of coarse sand with gravel (angular and sub-angular) and silty sand, gradually transitioning upwards to fine silt and silty clay, exhibiting poor sorting. The C–M (Cailleux–Middleton) diagram indicates an overwhelming dominance of the rolling component and sediment accumulates rapidly, reflecting strong tectonic subsidence control in the depositional basin. In the middle Pleistocene, the sediment in the stratigraphic sequence shifts from gravelly sand to upper clayey silty sand, with sporadic occurrences of foraminifera and ostracods in marine facies. The C–M diagram reflects sedimentation processes involving rolling, jumping, and suspension mixing, showing improved sorting. The sediment transport distance between the source and sink increases, reflecting a fluvial environment formed during the processes of peneplanation. From the late Pleistocene to the Holocene, there was a significant increase in the thickness of fine-grained strata, with improved sorting. The C–M diagram shows dominance of jumping and suspension, with a gradual disappearance of the rolling component. The sediment transport distance between the source and sink continued to increase. The strata reveal abundant marine foraminifera and marine ostracods, indicating the development of estuarine, shallow marine, and deltaic facies. This suggests frequent marine influence in the deltaic region during this period, with the topography significantly lower than in the earlier stages, approaching present-day elevation [43,44].

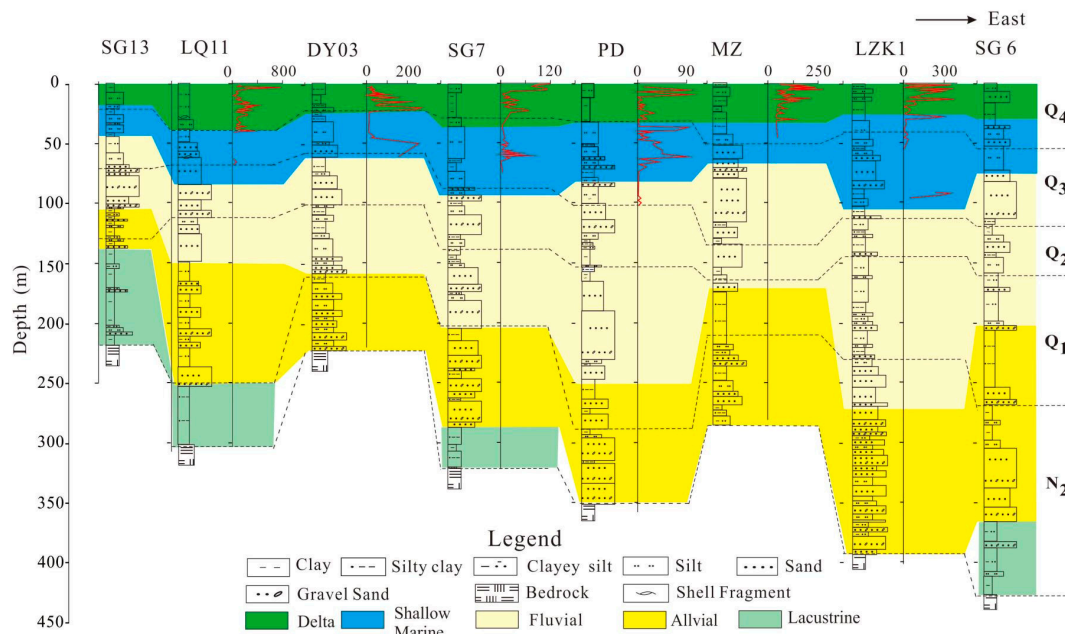


**Figure 8.** Sedimentary facies changes and the abundance of foraminifera (No./50 g) of sediment cores in the Yangtze Delta.

Gradual tectonic subsidence also occurred in the nearby Zhe-Min uplift on the East China Sea shelf during the Quaternary period [45,46]. With the subsidence of those regions, the main river channel shifted gradually from north to south, thus inducing a southward migration of depocenter beginning from the early Pleistocene (Figure 9). The mega-chrono-

stratigraphic cycle of cores implies not only the local sedimentary evolution of the Yangtze coast but also a hint of the channelization time of the Yangtze River.

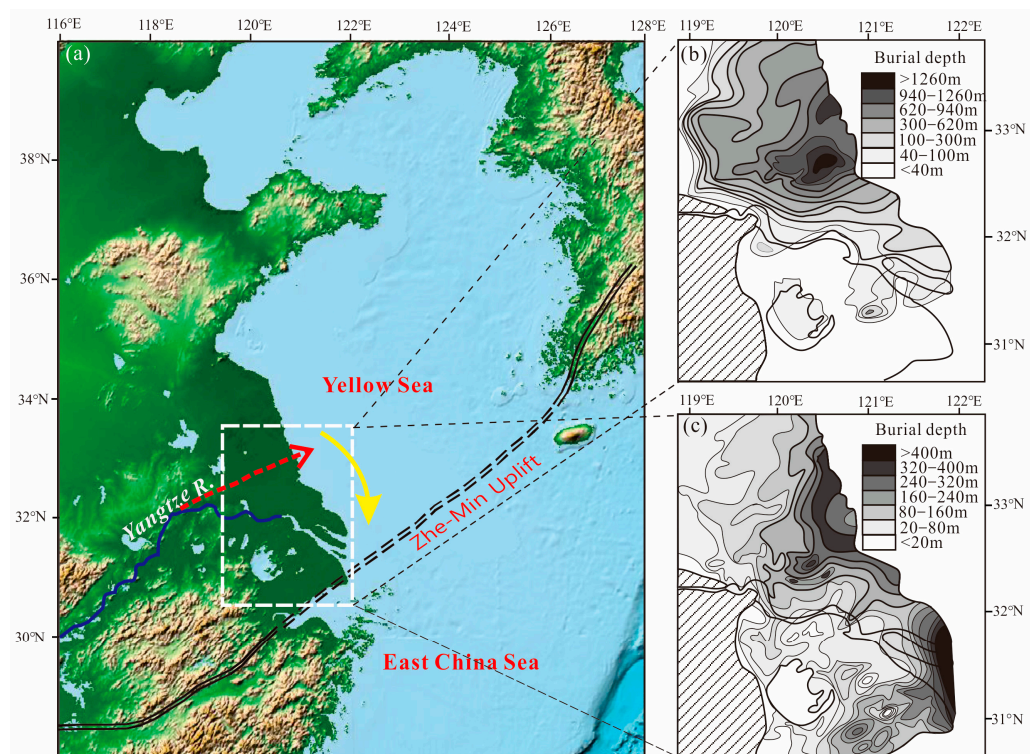


**Figure 9.** (a) Geomorphology in the Eastern Coastal Area of China and a southward migration of river channel (yellow arrow). (b) Neogene sedimentary thickness of the Yangtze Delta and Subei basin, modified after [18]. (c) Quaternary sedimentary thickness of the Yangtze Delta and Subei basin, modified after [18].

## 6. Conclusions

Magnetic properties combined with particle size, SEM observations, and EDS of the Pliocene red clay in the Yangtze Delta were analysed to reveal the paleoclimate and paleoenvironment of the East China coast. Based on the results of this study, we can reach the following conclusions: (1) the magnetic minerals of sediments are derived from the soil in local catchments, and the magnetic properties are generally controlled by the pedogenic intensity. (2) The Pliocene red clay generally has high S-ratios and low HIRM values, suggesting low pedogenesis intensity in the Pliocene. (3) High altitude constrained the chemical weathering and pedogenesis of Pliocene red clay and limited the transformation from pedogenic maghemite to haematite. Our results demonstrate a rapid tectonic subsidence occurring on the eastern China coast during the Quaternary era.

**Author Contributions:** X.L.: designed the research study and wrote the manuscript; J.C.: designed the research study; L.T.: conducted the fieldwork and measurements; M.L.: conducted the fieldwork and measurements; L.X.: analysed the data; X.S.: analysed the magnetic data; J.S.: designed the research study and reviewed the manuscript. All authors have read and agreed to the published version of the manuscript.

**Funding:** This research was funded by the National Science Foundation of China (Grant No. 41901102) and the Natural Science Foundation of Shandong Province, China (No. ZR2019PD013, ZR2019MD009).

**Institutional Review Board Statement:** Not applicable.

**Informed Consent Statement:** Not applicable.

**Data Availability Statement:** The data presented in this study are available on request from the corresponding author.

**Acknowledgments:** We would like to sincerely thank Baocheng Zhao for their help with field sampling, and Zhongyuan Chen for his helpful suggestions on the manuscript.

**Conflicts of Interest:** The authors declare no conflicts of interest.

## References

- An, Z.; Kutzbach, J.E.; Prell, W.L.; Porter, S.C. Evolution of Asian monsoons and phased uplift of the Himalaya-Tibetan plateau since Late Miocene times. *Nature* **2001**, *411*, 62–66.
- Guo, Z.; Ruddiman, W.F.; Hao, Q.; Wu, H.; Qiao, Y.; Zhu, R.; Peng, S.; Wei, J.; Yuan, B.; Liu, T. Onset of Asian desertification by 22 Myr ago inferred from loess deposits in China. *Nature* **2002**, *416*, 159–163. [[CrossRef](#)] [[PubMed](#)]
- Peng, W.; Zhang, H.; Pullen, A.; Li, M.; Pan, B.; Xiao, W.; Nie, J. Stepwise increased spatial provenance contrast on the Chinese loess plateau over late Miocene-Pleistocene. *Commun. Earth Environ.* **2023**, *4*, 60. [[CrossRef](#)]
- Hu, X.; Zhao, J.; Zhang, P.; Xue, Y.; Liu, X. Fe isotopic composition of the Quaternary red clay in subtropical Southeast China: Redoxic Fe mobility and its paleoenvironmental implications. *Chem. Geol.* **2019**, *524*, 356–367. [[CrossRef](#)]
- Qiao, Y.; Guo, Z.; Hao, Q.; Wu, W.; Jiang, W.; Yuan, B.; Zhang, Z.; Wei, J.; Zhao, H. Loess-soil sequences in south Anhui Province: Magnetostratigraphy and paleoclimatic significance. *China. Sci. Bull.* **2003**, *48*, 2088–2093. [[CrossRef](#)]
- Liu, C.; Zheng, L.; Wei, W.; Xu, X.; Sheng, H.; Yuan, B. Mineral magnetism to probe into the nature of palaeomagnetic signals of subtropical red soil sequences in southern China. *Geophys. J. Int.* **2010**, *18*, 1395–1410. [[CrossRef](#)]
- Thompson, R. *Environmental Magnetism*; Springer Science & Business Media: Berlin/Heidelberg, Germany, 1986.
- Liu, Q.; Roberts, A.P.; Larrasoana, J.C.; Banerjee, S.K.; Guyodo, Y.; Tauxe, L.; Oldfield, F. Environmental magnetism: Principles and applications. *Rev. Geophys.* **2012**, *50*, 1–124. [[CrossRef](#)]
- Kasbohm, J.; Schoene, B.; Montanari, A.; Coccioni, R. High-precision U-Pb zircon geochronology of the Miocene Bisciaro Formation, Contessa Section, Italy: A case study for requisite radioisotopic calibration of bio- and magnetostratigraphy. *Palaeogeogr. Palaeoclimatol. Palaeocol.* **2021**, *576*, 110487. [[CrossRef](#)]
- Zheng, Y.; Qiu, Z.; Qiu, Z.; Li, L.; Wei, X.; Zhang, R.; Yue, L.; Deng, T. Revised magnetostratigraphy of the Linxia Basin in the northeast Tibetan Plateau, constrained by micromammalian fossils. *Palaeogeogr. Palaeoclimatol. Palaeocol.* **2023**, *623*, 111620. [[CrossRef](#)]
- Lazos, I.; Sboras, S.; Chousianitis, K.; Kondopoulou, D.; Pikridas, C.; Bitharis, S.; Pavlides, S. Temporal evolution of crustal rotation in the Aegean region based on primary geodetically-derived results and palaeomagnetism. *Acta Geod. Geophys.* **2022**, *57*, 317–334. [[CrossRef](#)]
- Nie, J.; Song, Y.; King, J. A review of recent advances in red-clay environmental magnetism and paleoclimate history on the Chinese Loess Plateau. *Front. Earth Sci.* **2016**, *4*, 1–13. [[CrossRef](#)]
- Wang, S.; Lin, S.; Lu, S. Rock magnetism, iron oxide mineralogy and geochemistry of Quaternary red earth in central China and their paleopedogenic implication. *Palaeogeography, Palaeoclimatology, Palaeoecology* **2013**, *379*, 95–103. [[CrossRef](#)]
- Liu, C.; Wei, W.; Deng, C. A new weathering indicator from high-temperature magnetic susceptibility measurements in an Argon atmosphere. *Geophys. J. Int.* **2020**, *221*, 2010–2025. [[CrossRef](#)]
- Nie, J.; Zhang, R.; Necula, C.; Heslop, D.; Liu, Q.; Gong, L.; Banerjee, S. Late Miocene–early Pleistocene paleoclimate history of the Chinese Loess Plateau revealed by remanence unmixing. *Geophys. Res. Lett.* **2014**, *41*, 2163–2168. [[CrossRef](#)]
- Wang, S.; Lu, S. A rock magnetic study on red palaeosols in Yun-Gui Plateau (Southwestern China) and evidence for uplift of Plateau. *Geophys. J. Int.* **2014**, *196*, 736–747. [[CrossRef](#)]
- Hong, H.; Fang, Q.; Churchman, G.J.; Zhao, L.; Ji, K.; Jin, X.; Yin, K.; Wang, C.; Liu, C. Study of organic-matter intercalated vermiculitic phases in the hydromorphic red clay sediments. *Appl. Clay Sci.* **2020**, *196*, 105744. [[CrossRef](#)]
- Chen, Z.; Zong, Y.; Wang, Z.; Wang, H.; Chen, J. Migration patterns of Neolithic settlements on the abandoned Yellow and Yangtze River deltas of China. *Quat. Res.* **2008**, *70*, 301–314. [[CrossRef](#)]
- Liu, X.; Chen, J.; Maher, B.A.; Zhao, B.; Yue, W.; Sun, Q.; Chen, Z. Connection of the proto-Yangtze River to the East China Sea traced by sediment magnetic properties. *Geomorphology* **2018**, *303*, 162–171. [[CrossRef](#)]
- Roberts, A.P.; Pike, C.R.; Verosub, K.L. First-order reversal curve diagrams: A new tool for characterizing the magnetic properties of natural samples. *J. Geophys. Res.* **2000**, *105*, 28461–28475. [[CrossRef](#)]
- Chen, J.; Wang, Z.; Chen, Z.; Wei, Z.; Wei, T.; Wei, W. Diagnostic heavy minerals in Plio–Pleistocene sediments of the Yangtze delta, China with special reference to the Yangtze River connection to the sea. *Geomorphology* **2009**, *113*, 129–136. [[CrossRef](#)]
- Yue, W.; Liu, J.; Zhang, D.; Wang, Z.; Zhao, B.; Chen, Z.; Chen, J. Magnetite with anomalously high Cr<sub>2</sub>O<sub>3</sub> as a fingerprint to trace upper Yangtze sediments to the sea. *Geomorphology* **2016**, *268*, 14–20. [[CrossRef](#)]
- Sheldon, N.D.; Tabor, N.J. Quantitative paleoenvironmental and paleoclimatic reconstruction using paleosols. *Earth Sci. Rev.* **2009**, *95*, 1–52. [[CrossRef](#)]
- Hao, Q.; Guo, Z.; Qiao, Y.; Xu, B.; Oldfield, F. Geochemical evidence for the provenance of middle Pleistocene loess deposits in southern China. *Quat. Sci. Rev.* **2010**, *29*, 3317–3326. [[CrossRef](#)]

25. Barrón, V.; Torrent, J.; De Grave, E. Hydromaghemite, an intermediate in the hydrothermal transformation of 2-line ferrihydrite into hematite. *Am. Mineral.* **2003**, *88*, 1679–1688. [[CrossRef](#)]
26. Hu, P.; Liu, Q.; Torrent, J.; Barrón, V.; Jin, C. Characterizing and quantifying iron oxides in Chinese loess/paleosols: Implications for pedogenesis. *Earth Planet. Sci. Lett.* **2013**, *369*, 271–283. [[CrossRef](#)]
27. Torrent, J.; Barrón, V.; Liu, Q. Magnetic enhancement is linked to and precedes hematite formation in aerobic soil. *Geophys. Res. Lett.* **2006**, *33*, 140–165. [[CrossRef](#)]
28. Liu, C.; Deng, C.; Liu, Q. Mineral magnetic studies of the vermiculated red soils in southeast China and their paleoclimatic significance. *Palaeogeogr. Palaeoclimatol. Palaeocol.* **2012**, *329*, 173–183. [[CrossRef](#)]
29. Ji, R.; Hu, Z.; Zhang, W. Magnetic properties of the Jieshou red clay sequence in the Jinhua-Quzhou Basin, Southeastern China and its paleoenvironmental implications. *Quat. Sci.* **2015**, *35*, 1020–1029. (In Chinese)
30. Yin, Q.; Guo, Z. Mid-Pleistocene vermiculated red soils in southern China as an indication of unusually strengthened East Asian monsoon. *China Sci. Bull.* **2006**, *51*, 213–220. [[CrossRef](#)]
31. Zhao, Z.; Qiao, Y.; Wang, Y.; Fu, J.; Wang, S.; Li, C.; Yao, H.; Jiang, F. Can the magnetic susceptibility record of Chinese red clay sequence be used for palaeomonsoon reconstructions? *Geophys. J. Int.* **2016**, *204*, 1421–1429.
32. Zhang, W.; Yu, L.; Lu, M.; Zheng, X.; Shi, Y. Magnetic properties and geochemistry of the Xiashu Loess in the present subtropical area of China, and their implications for pedogenic intensity. *Earth Planet. Sci. Lett.* **2007**, *260*, 86–97. [[CrossRef](#)]
33. Liu, C.; Dupont-Nivet, G.; Wang, W.; Deng, C. Magnetic response to pedogenesis in aerobic soils of different weathering degree. *Palaeogeogr. Palaeoclimatol. Palaeocol.* **2021**, *567*, 1978–2012. [[CrossRef](#)]
34. Jenny, H. *Factors of Soil Formation: A System of Quantitative Pedology*; Courier Corporation: North Chelmsford, MA, USA, 1994.
35. Song, Y.; Fang, X.; Chen, X.; Torii, M.; Ishikawa, N.; Zhang, M.; Yang, S.; Chan, H. Rock magnetic record of late Neogene red clay sediments from the Chinese Loess Plateau and its implications for East Asian monsoon evolution. *Palaeogeogr. Palaeoclimatol. Palaeocol.* **2018**, *510*, 109–123. [[CrossRef](#)]
36. Wan, S.; Li, A.; Clift, P.D.; Jiang, H. Development of the East Asian summer monsoon: Evidence from the sediment record in the South China Sea since 8.5 Ma. *Palaeogeogr. Palaeoclimatol. Palaeocol.* **2006**, *241*, 139–159. [[CrossRef](#)]
37. Gai, C.; Liu, Q.; Roberts, A.P.; Chou, Y.; Zhao, X.; Jiang, Z.; Liu, J. East Asian monsoon evolution since the late Miocene from the South China Sea. *Earth Planet. Sci. Lett.* **2019**, *530*, 115960. [[CrossRef](#)]
38. Wang, H.; Lu, H. Climate controls on evolution of grassland ecosystems since late Cenozoic: A phytolith perspective. *Earth Sci. Rev.* **2022**, 104059. [[CrossRef](#)]
39. Zachos, J.; Pagani, M.; Sloan, L.; Thomas, E.; Billups, K. Trends, rhythms, and aberrations in global climate 65 Ma to present. *Science* **2001**, *292*, 686–693. [[CrossRef](#)] [[PubMed](#)]
40. Clemens, S.C.; Prell, W.L.; Sun, Y.; Liu, Z.; Chen, G. South Hemisphere forcing of Pliocene  $\delta^{18}\text{O}$  and the evolution of Indo-Asian monsoons. *Paleoceanography* **2008**, *23*, 1–15. [[CrossRef](#)]
41. Sun, Y.; An, Z.; Clemens, S.C.; Bloemendal, J.; Vandenberghe, J. Seven million years of wind and precipitation variability on the Chinese Loess Plateau. *Earth Planet. Sci. Lett.* **2010**, *297*, 525–535. [[CrossRef](#)]
42. Tian, J.; Xie, X.; Ma, W.; Jin, H.; Wang, P. X-ray fluorescence core scanning records of chemical weathering and monsoon evolution over the past 5 Myr in the south Southern China Sea. *Paleoceanography* **2011**, *26*, 1–17. [[CrossRef](#)]
43. Xiong, S.; Ding, Z.; Zhu, Y.; Zhou, R.; Lu, H. A~6Ma chemical weathering history, the grain size dependence of chemical weathering intensity, and its implications for provenance change of the Chinese loess–red clay deposit. *Quat. Sci. Rev.* **2010**, *29*, 1911–1922. [[CrossRef](#)]
44. Qiu, J.; Li, X. *Quaternary Stratigraphy and Sedimentary Environment of Shanghai*; Shanghai Science and Technology Press: Shanghai, China, 2007; pp. 1–230. (In Chinese)
45. Liu, J.; Zhang, X.; Mei, X.; Zhao, Q.; Guo, X.; Zhao, W.; Liu, J.; Saito, Y.; Wu, Z.; Li, J.; et al. The sedimentary succession of the last ~ 3.50 Myr in the western south Yellow Sea: Paleoenvironmental and tectonic implications. *Mar. Geol.* **2018**, *399*, 47–65. [[CrossRef](#)]
46. Yi, L.; Ye, X.; Chen, J.; Li, Y.; Long, H.; Wang, X.; Du, J.; Zhao, S.; Deng, C. Magnetostratigraphy and luminescence dating on a sedimentary sequence from northern East China Sea: Constraints on evolutionary history of eastern marginal seas of China since the Early Pleistocene. *Quat. Int.* **2014**, *349*, 316–326. [[CrossRef](#)]

**Disclaimer/Publisher’s Note:** The statements, opinions and data contained in all publications are solely those of the individual author(s) and contributor(s) and not of MDPI and/or the editor(s). MDPI and/or the editor(s) disclaim responsibility for any injury to people or property resulting from any ideas, methods, instructions or products referred to in the content.